# STRUCTURED INPUT-OUTPUT ANALYSIS OF OBLIQUE TURBULENT BANDS IN TRANSITIONAL PLANE COUETTE-POISEUILLE FLOW

### Yu Shuai

Dept. of Mechanics & Eng. Sci. Peking University Beijing, 100871, China 1800011056@pku.edu.cn

# **Chang Liu**

Dept. of Physics University of California, Berkeley Berkeley, CA, 94720, USA chang\_liu@berkeley.edu

## Dennice F. Gayme

Dept. of Mechanical Eng. Johns Hopkins University Baltimore, MD, 21218, USA dennice@jhu.edu

## **ABSTRACT**

In this work, we apply structured input-output analysis to study optimal perturbations and dominant flow patterns in transitional plane Couette-Poiseuille flow. The results demonstrate that this approach predicts the high structured gain of perturbations with wavelengths corresponding to the oblique turbulent bands observed in experiments. The inclination angles of these structures and their Reynolds number dependence are also consistent with previously observed trends. Reynolds number scalings of the maximally amplified structures for an intermediate laminar profile that is equally balanced between plane Couette and Poiseuille flow show an exponent that is at the midpoint of previously computed values for these two flows. However, the dependence of these scaling exponents on the shape of laminar flow as the relative contribution moves from predominately plane Couette to Poiseuille flow is not monotonic and our analysis indicates the emergence of different optimal perturbation structures through the parameter regime. Finally we adapt our approach to estimate the advection speeds of oblique turbulent bands in plane Couette flow and Poiseuille flow by computing their phase speed. The results show good agreement with prior predictions of the convection speeds of these structures from direct numerical simulations, which suggests that this framework has further potential in examining the dynamics of these structures.

## INTRODUCTION

A coexistence of turbulent and laminar behavior has been observed in wall-bounded shear flows as they transition from a laminar to a turbulent regime (Tuckerman *et al.*, 2020). This transitional state has been observed to take the form of bands of laminar and turbulent regions that form an oblique angle with the streamwise direction (Prigent *et al.*, 2003; Kanazawa, 2018). Numerical simulations (Tuckerman & Barkley, 2011; Tuckerman *et al.*, 2014; Fukudome & Iida, 2012) and experiments (Prigent *et al.*, 2003) have indicated that both the wavelengths and inclination angles of these structures are Reynolds number dependent. The sensitivity of the flow to perturbations of this type has been exploited through the use of these flow patterns as initial conditions to trigger turbulence in direct numerical simulations (DNS) (Tao *et al.*, 2018).

While the prevalence and large amplification of oblique turbulent bands in transitional wall-bounded shear flows has been widely observed, a comprehensive understanding of their underlying dynamics and role in transition has yet to be realized. Study of these structures is complicated by the very large channel size ( $\sim O(100)$  channel half-heights) required to observe them, see e.g., (Prigent *et al.*, 2002; Tuckerman & Barkley, 2011; Kim *et al.*, 2020). Computations of exact

coherent structures in channel flows also highlight the large domain sizes required to characterize the laminar-turbulent interface of these flow patterns (Schneider *et al.*, 2010). These large channel extents increase the computational costs of DNS and complexity of experiments needed to further study these structures.

Input-output analysis of the linearized Navier-Stokes (LNS) equations (Jovanović & Bamieh, 2005) provides a computationally tractable tool that has shown promise in analyzing transitional wall-bounded shear flows. In particular, the recently introduced *structured* input-output analysis has been shown to predict large amplification of similar oblique structures in transitional plane Couette and Poiseuille flow (Liu & Gayme, 2021). Both the large energy growth and features of the structures identified show good agreement with results from experiments (Prigent *et al.*, 2003) and DNS (Kanazawa, 2018), as well as predictions of nonlinear optimal perturbation analysis (Rabin *et al.*, 2012; Farano *et al.*, 2015).

In this work we apply structured input-output analysis to transitional plane Couette-Poiseuille flow (CPF). We first focus on the well studied intermediate case in which the shear and pressure gradient are equally weighted (Klotz et al., 2017a; Klotz & Wesfreid, 2017b; Klotz et al., 2021; Liu et al., 2021). Our results indicate that the oblique laminar-turbulent patterns with nonzero streamwise and spanwise wavenumbers show the highest gain under structured amplification. The wavelengths of the oblique turbulent bands identified are consistent with recent experimental observations (Klotz et al., 2021). In addition, the dependence of the predicted inclination angles on Reynolds number corresponds to previous findings in experiments of plane Couette flow (Prigent et al., 2003). We then analyze the how the Reynolds number scaling  $\sim O(Re^{\alpha})$ changes as a function of the shape of laminar base flow. The scaling of the highest structured gain for the intermediate flow regime is shown to be  $\alpha = 1.3$ , which is halfway between the respective values of  $\alpha = 1.1$  for plane Couette flow and 1.5 for plane Poiseuille flow found in Liu & Gayme (2021). However, the overall trends are not monotonic and the shape of the curve appears to suggest changes in the most amplified flow structures as the flow moves from background shear to pressure gradient dominant.

Finally, we show that the structured-input output method can be adapted to estimate the downstream advection speed of the oblique turbulent bands in plane Couette and Poiseuille flow. The results compare favorably to measurements based on oblique turbulent bands captured in DNS (Xiao & Song, 2020; Tuckerman *et al.*, 2014; Lu *et al.*, 2019). The combined analysis demonstrates the wide range of quantities that can be characterized by structured input-output analysis.

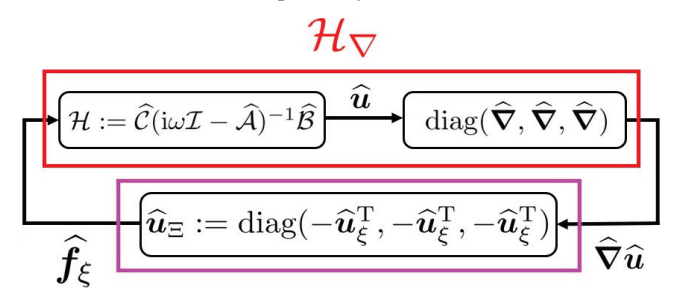


Figure 1. Illustration of the structured feedback interconnection between the modified frequency response operator  $\mathscr{H}_{\nabla} := \operatorname{diag}(\widehat{\boldsymbol{\nabla}},\widehat{\boldsymbol{\nabla}},\widehat{\boldsymbol{\nabla}})\mathscr{H}$  (blocks inside of red solid line –) and the structured uncertainty  $\widehat{\boldsymbol{u}}_{\Xi} := \operatorname{diag}(-\widehat{\boldsymbol{u}}_{\xi}^T, -\widehat{\boldsymbol{u}}_{\xi}^T, -\widehat{\boldsymbol{u}}_{\xi}^T)$  (block inside of purple solid line –). The modeled forcing term  $\widehat{\boldsymbol{f}}_{\xi} := [\widehat{f}_{x,\xi},\widehat{f}_{y,\xi},\widehat{f}_{z,\xi}]^T := \widehat{\boldsymbol{u}}_{\Xi}\widehat{\boldsymbol{\nabla}}\widehat{\boldsymbol{u}}$ , where  $\widehat{\boldsymbol{\nabla}}\widehat{\boldsymbol{u}} := [(\widehat{\boldsymbol{\nabla}}\widehat{\boldsymbol{u}})^T,(\widehat{\boldsymbol{\nabla}}\widehat{\boldsymbol{v}})^T]^T$  is the 9-by-1 vectorized velocity gradient.

#### **PROBLEM SETUP**

We consider incompressible flow between two infinite parallel plates with streamwise, wall-normal, spanwise and time coordinates (x,y,z,t), respectively. The total velocity is decomposed into a laminar base flow and fluctuations about that base flow, i.e.,  $\mathbf{u}_{tot} = [U(y),0,0]^T + \mathbf{u}$ . The pressure is similarly decomposed as  $p_{tot} = P + p$ . We employ the laminar base flow from Klotz & Wesfreid (2017b), which is given by

$$U(y) = \frac{3(1+\eta)}{4}(y^2 - 1) + \frac{1-\eta}{2}(y - 1) + 1.$$
 (1)

The parameter  $\eta \in [-1,1]$  determines the relative contribution of shear versus pressure gradient with  $\eta = -1$  corresponding to plane Couette flow with laminar profile U(y) = y, and  $\eta = 1$  to plane Poiseuille flow with  $U(y) = 1.5y^2 - 0.5$ . Here, the streamwise velocity is normalized by the upper-plate speed  $U^*$ , and length is normalized by the channel half-height h; leading to a wall-normal domain of  $y \in [-1,1]$  and Reynolds number  $Re := \frac{U^*h}{v}$ , where v denotes the kinematic viscosity.

The dynamics of velocity fluctuations  $\boldsymbol{u} := [u, v, w]^{\mathrm{T}}$  are governed by the Navier-Stokes equations (NSE). Following Liu & Gayme (2021) we linearize the NSE about the laminar based flow and treat the nonlinear terms as forcing  $\boldsymbol{f} := -\boldsymbol{u} \cdot \nabla \boldsymbol{u} = [f_x, f_y, f_z]^{\mathrm{T}}$ , which we model as

$$\boldsymbol{f}_{\xi} := \begin{bmatrix} -\boldsymbol{u}_{\xi}^{\mathrm{T}} \\ -\boldsymbol{u}_{\xi}^{\mathrm{T}} \\ -\boldsymbol{u}_{\xi}^{\mathrm{T}} \end{bmatrix} \begin{bmatrix} \boldsymbol{\nabla} \boldsymbol{u} \\ \boldsymbol{\nabla} \boldsymbol{v} \\ \boldsymbol{\nabla} \boldsymbol{w} \end{bmatrix} = \begin{bmatrix} f_{x,\xi} \\ f_{y,\xi} \\ f_{z,\xi} \end{bmatrix}. \tag{2}$$

This model preserves the structure of the nonlinear interactions of the NSE since all elements outside of the block-diagonal elements  $\mathrm{diag}(-\boldsymbol{u}_{\xi}^{\mathrm{T}},-\boldsymbol{u}_{\xi}^{\mathrm{T}},-\boldsymbol{u}_{\xi}^{\mathrm{T}})$  are zero.

We employ the standard transformation to write the governing equations in terms of the fluctuating wall-normal velocity and vorticity  $[v, \omega_y]^T$ . We then perform the triple Fourier transform  $\widehat{(\cdot)}(y; k_x, k_z, \omega) := \int_{-\infty}^{\infty} \int_{-\infty}^{\infty} (\cdot)(x, y, z, t) e^{-i(k_x x + k_z z + \omega t)} dx dz dt$ . Here  $k_x$  and  $k_z$  are the respective streamwise and spanwise wavenumbers,  $\omega$  is the frequency and  $i = \sqrt{-1}$ . The transformed linearized NSE driven by the modeled forcing  $\hat{\boldsymbol{f}}_\xi$  for each  $(k_x, k_z, \omega)$  triplet is then given by

$$i\omega \begin{bmatrix} \widehat{v} \\ \widehat{\omega}_{y} \end{bmatrix} = \widehat{\mathscr{A}} \begin{bmatrix} \widehat{v} \\ \widehat{\omega}_{y} \end{bmatrix} + \widehat{\mathscr{B}} \begin{bmatrix} \widehat{f}_{x,\xi} \\ \widehat{f}_{y,\xi} \\ \widehat{f}_{z,\xi} \end{bmatrix}, \tag{3a}$$

$$\begin{bmatrix} \widehat{u} \\ \widehat{v} \\ \widehat{w} \end{bmatrix} = \widehat{\mathscr{C}} \begin{bmatrix} \widehat{v} \\ \widehat{\omega}_{y} \end{bmatrix}, \tag{3b}$$

where (Jovanović & Bamieh, 2005)

$$\begin{split} \widehat{\mathscr{A}} := & \mathscr{M}^{-1} \begin{bmatrix} -\mathrm{i} k_x U \widehat{\nabla}^2 + \mathrm{i} k_x U'' + \widehat{\nabla}^4 / Re & 0 \\ -\mathrm{i} k_z U' & -\mathrm{i} k_x U + \widehat{\nabla}^2 / Re \end{bmatrix}, \\ \widehat{\mathscr{B}} := & \mathscr{M}^{-1} \begin{bmatrix} -\mathrm{i} k_x \partial_y - (k_x^2 + k_z^2) & -\mathrm{i} k_z \partial_y \\ \mathrm{i} k_z & 0 & -\mathrm{i} k_x \end{bmatrix}, \; \mathscr{M} := \begin{bmatrix} \widehat{\nabla}^2 & 0 \\ 0 & \mathbb{I} \end{bmatrix} \\ \widehat{\mathscr{C}} := & \frac{1}{k_x^2 + k_z^2} \begin{bmatrix} \mathrm{i} k_x \partial_y & -\mathrm{i} k_z \\ k_x^2 + k_z^2 & 0 \\ \mathrm{i} k_z \partial_y & \mathrm{i} k_x \end{bmatrix}. \end{split}$$

We employ no-slip boundary conditions  $\widehat{v}(y=\pm 1) = \partial \widehat{v}/\partial y (y=\pm 1) = \widehat{\omega}_v (y=\pm 1) = 0$ .

We are interested in defining the block-diagonal gain operator  $\mathbf{u}_\Xi := \operatorname{diag}(-\mathbf{u}_\xi^T, -\mathbf{u}_\xi^T, -\mathbf{u}_\xi^T)$  that maximizes the response of the structured input-output system in Fig. 1. To build this feedback interconnection we define  $\mathscr{H}_\nabla := \operatorname{diag}(\widehat{\nabla}, \widehat{\nabla}, \widehat{\nabla})\mathscr{H}$ , where  $\mathscr{H}(y; k_x, k_z, \omega) := \widehat{\mathscr{C}}(\operatorname{i}\omega\mathbb{I} - \widehat{\mathscr{A}})^{-1}\widehat{\mathscr{B}}$  is the spatio-temporal frequency response operator mapping  $\widehat{f}_\xi$  to  $\widehat{u}$  for each triplet  $(k_x, k_z, \omega)$  and  $\mathbb{I}$  is the identity operator. The modified operator  $\mathscr{H}_\nabla$  maps  $\widehat{f}_\xi := [\widehat{f}_{x,\xi},\widehat{f}_{y,\xi},\widehat{f}_{z,\xi}]^T$  to the 9-by-1 vectorized velocity gradient  $\widehat{\nabla}\widehat{u} := [(\widehat{\nabla}\widehat{u})^T, (\widehat{\nabla}\widehat{v})^T, (\widehat{\nabla}\widehat{w})^T]^T$ . Defining this modified operator allows us to evaluate the closed-loop system defined by the feedback interconnection between  $\mathscr{H}_\nabla$  and the block-diagonal structured gain  $\widehat{u}_\Xi := \operatorname{diag}(-\widehat{u}_\xi^T, -\widehat{u}_\xi^T, -\widehat{u}_\xi^T)$  shown in Fig. 1.

We then define the structured input-output response (Liu & Gayme, 2021) as

$$\|\mathscr{H}_{\nabla}\|_{\mu}(k_{x},k_{z}) := \sup_{\omega \in \mathbb{R}} \mu_{\widehat{\boldsymbol{U}}_{\Xi}}[\mathbf{H}_{\nabla}(k_{x},k_{z},\omega)], \qquad (5)$$

where

$$\mu_{\widehat{\boldsymbol{U}}_{\Xi}}\left[\mathbf{H}_{\nabla}(\cdot)\right] := \begin{cases} \frac{1}{\min\{\bar{\sigma}\left[\widehat{\boldsymbol{u}}_{\Xi}\right]: \widehat{\boldsymbol{u}}_{\Xi} \in \widehat{\boldsymbol{U}}_{\Xi}, \det[\mathbb{I} - \mathbf{H}_{\nabla}(\cdot)\widehat{\boldsymbol{u}}_{\Xi}] = 0\}}, \\ 0, \text{if } \forall \; \widehat{\boldsymbol{u}}_{\Xi} \in \widehat{\boldsymbol{U}}_{\Xi}, \det\left[\mathbb{I} - \mathbf{H}_{\nabla}(\cdot)\widehat{\boldsymbol{u}}_{\Xi}\right] \neq 0 \end{cases}$$

is the structured singular value of  $\mathbf{H}_{\nabla}(k_x, k_z, \omega)$  for each triplet  $(k_x, k_z, \omega)$  (Packard & Doyle, 1993). Here  $\widehat{\boldsymbol{U}}_{\Xi} :=$ 

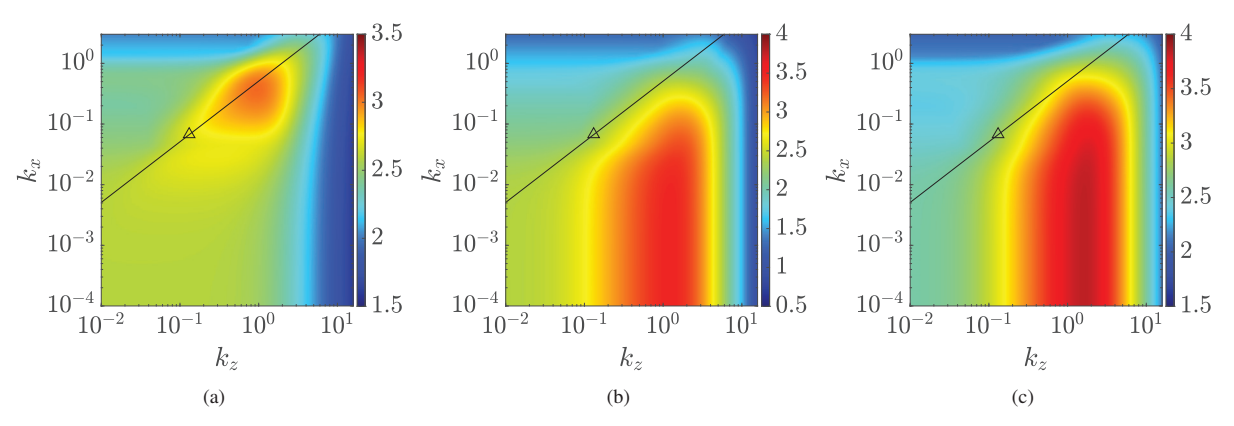


Figure 2. Contour plots of (a)  $\log_{10}[\|\mathcal{H}_{\nabla}\|_{\mu}(k_x,k_z)]$ , (b)  $\log_{10}[\|\mathcal{H}\|_{\infty}(k_x,k_z)]$  and (c)  $\log_{10}[\|\mathcal{H}_{\nabla}\|_{\infty}(k_x,k_z)]$  for plane Couette-Poiseuille flow  $U(y) = \frac{3}{4}(y^2 - 1) + \frac{1}{2}(y + 1)$  at Re = 610 and  $\eta = 0$ . Here, the black triangle ( $\Delta$ ) marks  $\lambda_x \approx 93$  and  $\lambda_z \approx 48$  which are the wavelengths of the observed oblique turbulent band at Re = 610 (Klotz *et al.*, 2021). The black solid line (-)  $\lambda_z = \lambda_x \tan(27^\circ)$  corresponds to a  $27^\circ$  oblique angle of the oblique turbulent band.

 $\{\mathrm{diag}(-\widehat{\mathbf{u}}_{\xi}^{\mathrm{T}},-\widehat{\mathbf{u}}_{\xi}^{\mathrm{T}},-\widehat{\mathbf{u}}_{\xi}^{\mathrm{T}}):-\widehat{\mathbf{u}}_{\xi}^{\mathrm{T}}\in\mathbb{C}^{N_{y}\times3N_{y}}\}$  is the set of wall-normally discretized structured uncertainties with the same block-diagonal structure as  $\widehat{\boldsymbol{u}}_{\Xi}$ , and  $N_{y}$  denotes the number of Chebyshev collocation points excluding boundary points.  $\mathbf{H}_{\nabla}$  denotes the discretized spatio-temporal frequency response operator,  $\bar{\boldsymbol{\sigma}}[\cdot]$  represents the largest singular value of the argument, and  $\det[\cdot]$  is the determinant of the argument.

#### **RESULTS**

In this section, we compute the response in (5) using MATLAB with Chebyshev differentiation matrices from Weideman & Reddy (2000). We employ  $N_y=30$  collocation points in the wall normal direction and  $50\times 90$  logarithmically spaced points in the spatial wavenumber domain  $k_x\in[10^{-4},10^{0.48}]$  and  $k_z\in[10^{-2},10^{1.2}]$ . This configuration matches that in Liu & Gayme (2021), who found this number of points sufficient for convergence of the results.

We first consider the intermediate case, the laminar profile with  $\eta = 0$  in (1), which corresponds to equal weighting of the contributions from plane Couette and Poiseuille flow. This profile is linearly stable for all Reynolds numbers (Balakumar, 1997). Fig. 2 (a) shows the corresponding  $\|\mathcal{H}_{\nabla}\|_{\mu}(k_x, k_z)$  at Re = 610, which was selected to match that in Klotz et al. (2021). Here, the peak region covers the wavelength range  $\lambda_x \approx 93 \pm 5$  and  $\lambda_z \approx 48 \pm 5$ . This region is consistent with the oblique turbulent bands observed in Klotz et al. (2021, Fig. 20), whose results are indicated as a black triangles ( $\Delta$ ) in all panels of Fig. 2. The shape of the peak region in Fig. 2(a) also reflects the same inclination angle  $\theta := \tan^{-1}(\lambda_z/\lambda_x) = \tan^{-1}(48/93) \approx 27^{\circ}$  (the black solid line in Fig. 2) as the experimentally observed band. The consistency of our results with the literature shows that structured input-output analysis captures both the length scales and inclination angles of dominant flow structures in this intermediate case of plane CPF.

We next compare these results to similar quantities that would be obtained through an unstructured analysis by computing  $\|\mathscr{H}\|_{\infty}(k_x,k_z) := \sup_{\omega \in \mathbb{R}} \bar{\sigma}\left[\mathbf{H}(k_x,k_z,\omega)\right]$  and  $\|\mathscr{H}_{\nabla}\|_{\infty}(k_x,k_z) := \sup_{\omega \in \mathbb{R}} \bar{\sigma}\left[\mathbf{H}_{\nabla}(k_x,k_z,\omega)\right]$ , respectively shown in Figs. 2(b) and (c). The figures show that both of these quantities place more emphasis on the streamwise elongated structures associated with  $k_x \approx 0$  than the oblique turbulent

bands. These results also indicate that the change in the response is due to the structured feedback interconnection rather than the modified frequency response operator. These differences between the structured and the traditional unstructured input-output response is similar to that seen in previous studies of plane Couette and Poiseuille flow, where the change in the structures obtained under the structured feedback interconnection was related to a weakening of the lift-up mechanism that dominates the unstructured response (Liu & Gayme, 2021).

We next study the inclination angles and length scales of structures that maximize the structured gain for this intermediate case ( $\eta=0$ ) and examine and their dependence on Reynolds number. We define this dominant angle as  $\theta=\tan^{-1}(k_x^M/k_z^M)$ , where  $k_x^M$  and  $k_z^M$  are defined as the wavenumbers associated with the largest structured gain

$$(k_x^M, k_z^M) := \underset{k_x, k_z}{\arg \max} \| \mathscr{H}_{\nabla} \|_{\mu} (k_x, k_z).$$
 (6)

Fig. 3(a) shows how these wavelengths vary as a function of Reynolds number. Here it is clear that while both wavenumbers decrease as Re increases,  $k_x^M$  decreases faster. We quantify this difference by computing scalings of these quantities with Reynolds number using a fit of the form of  $C_iRe^{\alpha_i}(i=1,2,3)$ . The results show that  $k_x^M \sim Re^{-0.41}$  and  $k_x^M \sim Re^{-0.34}$ . We note that this scaling of  $k_x^M$  is consistent with previous analysis in the optimal wavenumber range  $k_x \leq O(1)$  for oblique flow structures that produce streamwise vortices in wall-bounded shear flows (Chapman, 2002). These trends are consistent with a reduction in the inclination angle as a function of Reynolds number over this range.

Fig. 3(b) and (c) show  $\|\mathcal{H}_{\nabla}\|_{\mu}$  for two additional Reynolds numbers, respectively Re=2000 and 20000. In both panels the most energetic wavenumber pairs, respectively  $(k_x^M, k_z^M) = (0.25, 0.67)$  and (0.08, 0.29) are indicated with a black asterisk. These figures indicate that  $\theta$  decreases from approximately 22° to 15° over this Reynolds number range, and that both angles are lower than the value at Re=610. In addition, as Reynolds number increases, the peak response region extends visibly and shifts slightly more towards larger streamwise wavelengths than toward the large spanwise ones. This negative correlation is consistent with trends observed in previous studies of laminar-turbulent patterns in plane Couette flow (Prigent et al., 2003).

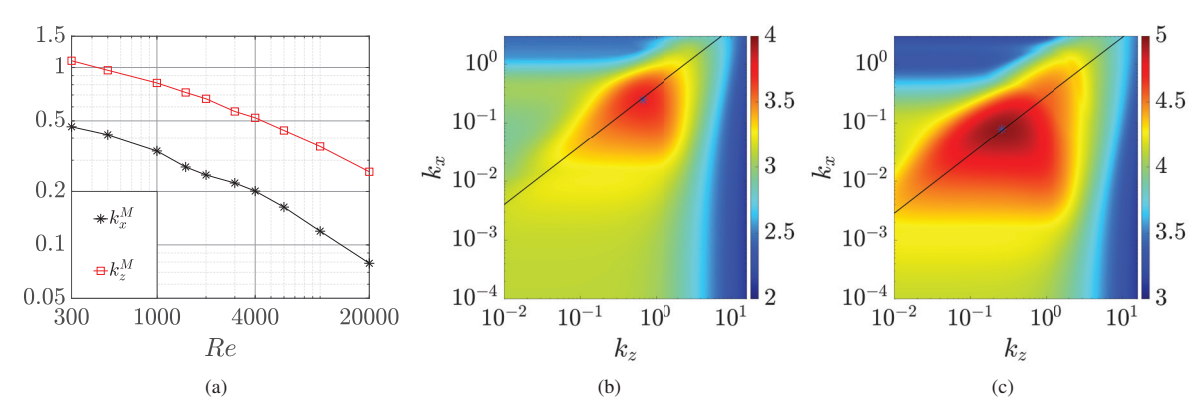


Figure 3. (a) The most energetic wavenumber pairs from Re=300 to 20000 with scalings  $k_x^M \sim Re^{-0.41}$  and  $k_z^M \sim Re^{-0.34}$  and contour plots showing the relative location of regions associated with peak structured frequency response at (b) Re=2000 and (c) 20000 with Re=2000 and (c) symbol the wavenumber pairs Re=2000 and Re=2000 and Re=2000 and Re=2000 are Re=2000 are Re=2000 and Re=2000 are Re=2000 are Re=2000 are Re=2000 and Re=2000 are Re=2000 are Re=2000 and Re=2000 are Re=2000 are Re=2000 and Re=2000 are Re=2000 are Re=2000 are Re=2000 and Re=2000 are Re=2000 and Re=2000 are Re=2000 and Re=2000 are Re=2000 and Re=2000 are Re=2000 are Re=2000 and Re=2000 are Re=2000 and Re=2000 are Re=2000 and Re=2000 are Re=2000 are Re=2000 and Re=2000 and Re=2000 are Re=2000 and Re=2000 are Re=2000 and Re=2000 are Re=2000 and Re=2000 are Re=2000 are Re=2000 and Re=2000 are Re=2000 are Re=2000 and Re=2000 are Re=2000 are Re=2000 and Re=2000 are Re=2000 and Re=2000 are Re=2000 and Re=2000 are Re=2000 are Re=2000 and Re=2000 are Re=2000 are Re=2000 are Re=2000 and Re=2000 are Re=2000 and Re=2000 are Re=2000 are Re=2000 and Re=2000 are Re=2000 are Re=2000 and Re=2000 are Re=2000 are Re=2000 are Re=2000 are Re=2000 are Re=2000 are Re=2000 and Re=2000 are Re=2000 ar

The maximal response for a given Reynolds number for the three quantities in Fig. 2 can be respectively quantified as  $\|\mathscr{H}_{\nabla}\|_{\mu}^{M} := \max_{k_{x},k_{z}} \|\mathscr{H}_{\nabla}\|_{\mu}(k_{x},k_{z}), \|\mathscr{H}_{\nabla}\|_{\infty}^{M} :=$  $\max_{k_x,k_z} \|\mathscr{H}_\nabla\|_\infty(k_x,k_z), \text{ and } \|\mathscr{H}\|_\infty^M := \max_{k_x,k_z} \|\mathscr{H}\|_\infty(k_x,k_z). \text{ These }$ quantities for the range  $Re \in [300,4000]$  are depicted in Fig. 4(a), where we again obtain their respective Reynolds number scalings through a fit to  $C_i Re^{\alpha_i} (i = 1, 2, 3)$ . The results reveal that both  $\|\mathcal{H}_{\nabla}\|_{\infty}^{M}$  and  $\|\mathcal{H}\|_{\infty}^{M}$  scale as  $Re^{2}$ , which is the same scaling seen in both plane Couette and Poiseuille flow, see e.g. Trefethen et al. (1993); Jovanović (2004). However,  $\|\mathscr{H}_{\nabla}\|_{\mu}^{M} \sim Re^{1.3}$ , and this lower scaling exponent ver-Sust the unstructured response is similar to previous results that showed  $\|\mathscr{H}_{\nabla}\|_{\mu}^{M} \sim Re^{1.1}$  for plane Couette flow U(y) = y and  $\|\mathscr{H}_{\nabla}\|_{\mu}^{M} \sim Re^{1.5}$  for plane Poiseuille flow  $U(y) = 1 - y^2$  (Liu & Gayme, 2021). This lower amplification of the structured response is consistent with previous observations that the structured feedback weakens the amplification of the lift-up mechanism in a manner similar to that of nonlinear effects in plane Couette and plane Poiseuille flows (Liu & Gayme, 2021).

We next explore how the scaling and structural features vary as a function of the relative contributions of shear and pressure gradient forcing to the laminar profile shape. Fig. 4(b) shows the scaling exponents of the maximal structured frequency response  $\|\mathscr{H}_{\nabla}\|_{\mu}^{M}\sim Re^{lpha}$  with laminar profiles defined by equation (1) with  $\eta = [-1, 1]$  computed at steps of 0.1 over the Reynolds number range  $Re \in [300, 4000]$ . Fig. 4(b) indicates that  $\alpha$  grows from 1.1 to 1.35 as  $\eta$  increases roughly from -1 to 0.3, and then declines at a low rate in the range  $0.3 \le \eta \le 0.7$  before finally climbing to  $\alpha = 1.5$ at  $\eta = 1$ . While the end points are consistent with previous scalings associated with plane Couette and Poiseuille flow, the non-monotonic growth of the scaling exponent was unexpected. In order to analyze this behavior we explore the structural features associated with the different regions of this scaling plot in Fig. 5, which shows  $\|\mathcal{H}_{\nabla}\|_{\mu}(k_x,k_z)$  for laminar profiles corresponding to  $\eta = -1, -0.5, 0, 0.3, 0.5, 0.7, 0.9$ and 1 for Re = 500.

Figs. 5 (a) – (c) indicate that there is a single peak frequency response region  $(k_x, k_z) \approx (10^{-1}, 1)$  associated with oblique flow structures when  $-1 \le \eta \le 0$ . In this region the

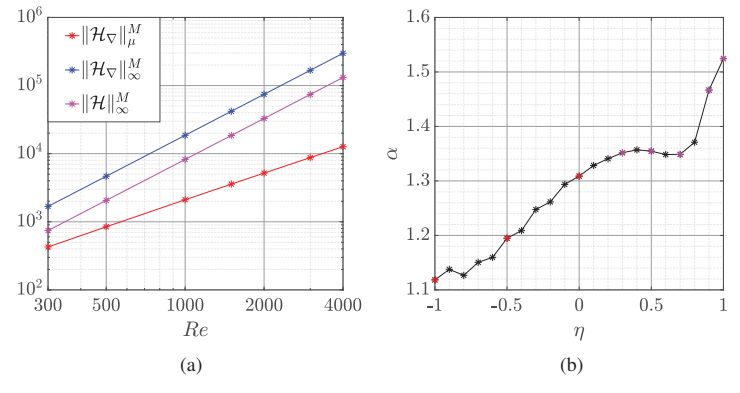


Figure 4. (a) Reynolds number dependence of the maximal structured and unstructured frequency response associated with scaling  $\|\mathscr{H}_{\nabla}\|_{\mu}^{M} \sim Re^{1.3}$ ,  $\|\mathscr{H}_{\nabla}\|_{\infty}^{M} \sim Re^{2}$  and  $\|\mathscr{H}\|_{\infty}^{M} \sim Re^{2}$  at  $Re \in [300,4000]$  and  $\eta = 0$ . (b) The dependence of scaling exponents  $\alpha$  in  $\|\mathscr{H}_{\nabla}\|_{\mu}^{M} \sim Re^{\alpha}$  on the parameter  $\eta$  determining the shape of laminar base flow  $U(y) = \frac{3(1+\eta)}{4}(y^{2}-1) + \frac{1-\eta}{2}(y-1) + 1$ . The asterisks in panel (b) represent  $\alpha$  at  $\eta = -1, -0.9, ..., 0.9, 1$ . The red asterisks (\*\*) mark  $\eta = -1, -0.5, 0$ , the magenta ones (\*\*) mark  $\eta = 0.3, 0.5, 0.7, 0.9, 1$ , and the black ones (\*\*) indicate the remaining values of  $\eta$ .

Table 1. Advection speeds *c* of laminar-turbulent patterns in plane Couette and Poiseuille flows by predictions of structured inputoutput analysis and results of direct numerical simulations. Here the paper sources where we obtain DNS results of advection speeds are consistent with those of wavenumbers in the third column.

Laminar	Reynolds	Wavenumbers	Estimations of c	DNS Results of c
Profile	Number	$(k_x,k_z)$ and	by Structured	and Their Sources
U(y)	Re	Their Sources	I/O Analysis	(From Papers in Col. 3)
$1 - y^2$	750	(0.15, 0.10) (Fig. 1(a), Xiao & Song, 2020)	0.92	0.85 (Fig. 1(b))
$\frac{1}{2} - \frac{3}{2}y^2$	1100	(0.06, 0.14) (Fig. 2(a), Tuckerman <i>et al.</i> , 2014)	$\approx 0$	0.07 (Fig. 4(b))
y	317	(0.04,0.05) (Fig. 3(b), Lu et al., 2019)	$\approx 0$	$\approx 0$ (Fig. 4)

scaling is increasing at a roughly constant rate and the angle associated with these structures appears to increase with  $\eta$ . Panels (d) – (h) indicate that a new wavenumber region  $(k_x, k_z) \approx (1,0)$  corresponding to large structured frequency response emerges in the slowly decreasing (roughly flat region in Fig. 4(b). Given that the laminar flow is no longer linearly stable for all Reynolds numbers for  $\eta$  > 0.309 (Balakumar, 1997), these are likely associated with the Tollmien-Schlichting (TS) waves that become unstable at higher Reynolds numbers. This conjecture is supported by the fact that the TS wavenumbers ranges are consistent with these regions. The definition of this secondary TS related peak becomes sharper for  $\eta > 0.7$  as does the peak range of the oblique structures. The angle associated with these structures and shape of this region also changes for  $\eta > 0.7$ , which may indicate a change in the characteristic structures in this parameter regime. A full characterization of how the structural features of the flow change with  $\eta$  is a direction of ongoing work.

Finally, we adapt the structured input-output approach to compute the phase speed associated with the maximum response, which we interpret as the convective velocity of these structures. We limit the analysis to the case where the temporal frequency  $\omega \in \mathbb{R}$ , since any time-dependent flow structure

can be represented by integrating its Fourier components over real temporal frequencies (Trefethen *et al.*, 1993). The phase speed c of a given oblique flow structure with  $(k_x, k_z) \neq 0$  is obtained as

$$c(k_x, k_z) = -\frac{1}{k_x} \arg \max_{\boldsymbol{\omega} \in \mathbb{R}} \mu_{\widehat{\boldsymbol{U}}_{\Xi}} \left[ \mathbf{H}_{\nabla}(k_x, k_z, \boldsymbol{\omega}) \right]. \tag{7}$$

In order to validate the approach we focus our investigation on the phase speeds of flow patterns in plane Couette and plane Poiseuille flow, which have been previously studied (Tuckerman *et al.*, 2014; Xiao & Song, 2020; Lu *et al.*, 2019). Table. I provides a comparison between the advection speeds of the laminar turbulent (oblique bands) predicted from our approach to results computed from the DNS of Lu *et al.* (2019); Tuckerman *et al.* (2014) and Xiao & Song (2020). The oblique turbulent band wavenumbers ( $k_x, k_z$ ) reported were extracted from snapshots of these DNS results, specifically from Lu *et al.*, 2019, Fig. 3 (b); Tuckerman *et al.*, 2014, Fig. 4 (a); Xiao & Song, 2020, Fig. 1 (a), respectively. In each case, the table indicates the laminar base flows and Reynolds numbers from the references. We note that Tuckerman *et al.* (2014) and Lu *et al.* (2019) use the same characteristic length and velocity

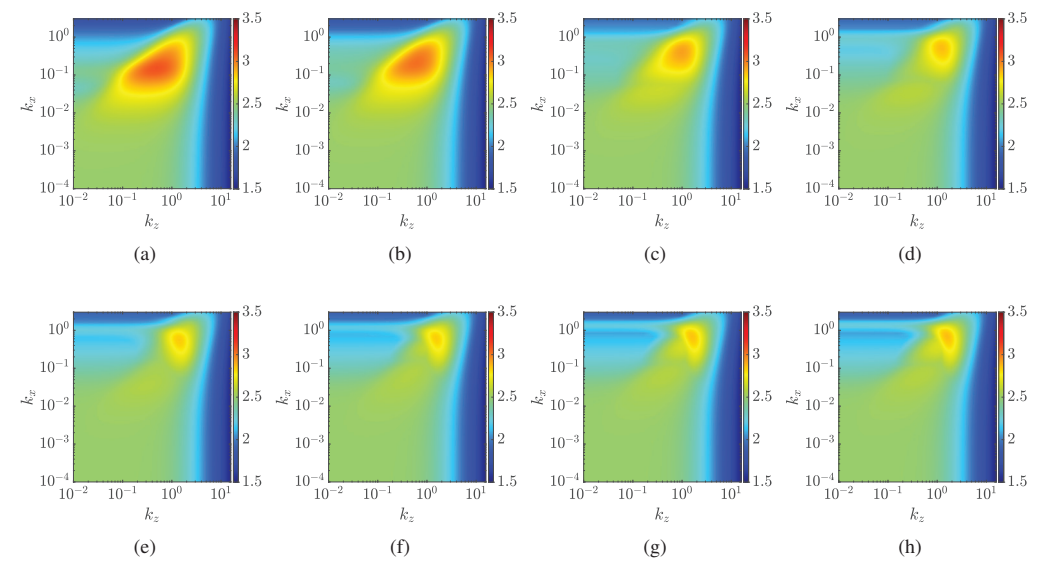


Figure 5. Plots of  $\log_{10}[\|\mathscr{H}_{\nabla}\|_{\mu}(k_x,k_z)]$  at Re = 500 with (a)  $\eta = -1$ , (b)  $\eta = -0.5$ , (c)  $\eta = 0$ , (d)  $\eta = 0.3$ , (e)  $\eta = 0.5$ , (f)  $\eta = 0.7$ , (j)  $\eta = 0.9$ , and (h)  $\eta = 1$ . The shape of laminar flow  $\eta$  associated with panels (a)–(c) correspond to the red asterisks (\*) while panels (d)–(h) match with the magenta asterisks (\*) in Fig. 4 (b).

scales as our analysis so their laminar profiles directly correspond to the cases where  $\eta=1$  and  $\eta=-1$  respectively, so we can directly compare to their results by matching the Reynolds numbers. On the other hand, the flow configuration in Lu *et al.* (2019) differs from ours, which leads to a different laminar profile. In order to compare with those results, we renormalize velocity using the centerline speed of base flow  $U_{cen}^*$  and redefine the laminar plane Poiseuille flow as  $U(y)=1-y^2$  and the Reynolds number as  $Re:=\frac{U_{cen}^*h}{v}$ .

The results in Table 1 indicate that the estimated values have a resonable margin of error when compared to the DNS results. This success in predicting the traveling speeds of the given structures indicates that our framework may be useful in estimating the convection rate of different flow structures. Although further analysis is needed to fully validate this approach for a wider range of structures, these preliminary results suggest the promise of this framework in probing the dynamics of the oblique turbulent bands.

#### **CONCLUSIONS**

In this paper, we apply structured input-output analysis to study the oblique turbulent bands that have been observed in transitional plane Couette-Poiseuille flow (CPF). The results reveal that the wavenumbers of these structure are associated with large gain under structured feedback forcing. As Reynolds number increases, these most energetic streamwise and spanwise wavenumbers decrease with different scalings  $k_r^M \sim Re^{-0.41}$  and  $k_z^M \sim Re^{-0.34}$ , thereby resulting in the decline of oblique angles and extension of the wavenumber region associated with the large response. The Reynolds number scaling of the maximal structured amplification  $\|\mathscr{H}_{\nabla}\|_{\mu}^{M}$ associated with dominant oblique patterns changes from 1.1 to 1.5 as the laminar profile changes from plane Couette flow to plane Poiseuille flow, with an intermediate CPF flow value of 1.3. While the end points are consistent with previous results and the intermediate flow falls at the midpoint the increase is not monotonic and the analysis suggests that different structural features emerge as the pressure gradient contribution to the laminar profile is increased. Further characterization of this behavior is a direction for future work.

Finally we adapt the framework to predict the advection speeds of oblique turbulent bands for plane Couette and Poiseuille flow configurations. The results are consistent with DNS and indicate the promise of this approach in further analyzing the dynamics of these transitional structures.

## **ACKNOWLEDGEMENTS**

The authors gratefully acknowledge partial support from the US National Science Foundation (CBET 1652244).

# **REFERENCES**

- Balakumar, P. 1997 Finite-amplitude equilibrium solutions for plane Poiseuille-Couette flow. *Theor. Comput. Fluid Dyn.* **9**, 103–119.
- Chapman, S. J. 2002 Subcritical transition in channel flows. *J. Fluid Mech.* **451**, 35–97.
- Farano, M., Cherubini, S., Robinet, J. C. & De Palma, P. 2015 Hairpin-like optimal perturbations in plane Poiseuille flow. J. Fluid Mech. 775, R2.
- Fukudome, K. & Iida, O. 2012 Large-scale flow structure in turbulent Poiseuille flows at low-Reynolds numbers. J. Fluid Sci. Tech. 7 (1), 181–195.

- Jovanović, M. R. 2004 Modeling, analysis, and control of spatially distributed systems. PhD thesis, University of California, Santa Barbara.
- Jovanović, M. R. & Bamieh, B. 2005 Componentwise energy amplification in channel flows. J. Fluid Mech. 534, 145– 183
- Kanazawa, T. 2018 Lifetime and growing process of localized turbulence in plane channel flow. PhD thesis, Osaka University.
- Kim, J. H., Hwang, J. H., Lee, Y. M. & Lee, J. H. 2020 Direct numerical simulation of a turbulent Couette-Poiseuille flow, part 2: Large- and very-large-scale motions. *Int. J. Heat Fluid Flow* 86, 108687.
- Klotz, L., Lemoult, G., Frontczak, I., Tuckerman, L. S. & Wesfreid, J. E. 2017a Couette-Poiseuille flow experiment with zero mean advection velocity: Subcritical transition to turbulence. *Phys. Rev. Fluids* 2, 043904.
- Klotz, L., Pavlenko, A. M. & Wesfreid, J. E. 2021 Experimental measurements in plane Couette-Poiseuille flow: dynamics of the large- and small-scale flow. J. Fluid Mech. 912, A24.
- Klotz, L. & Wesfreid, J. E. 2017b Experiments on transient growth of turbulent spots. J. Fluid Mech. 829, R4.
- Liu, C. & Gayme, D. F. 2021 Structured input-output analysis of transitional wall-bounded flows. J. Fluid Mech. 927, A25.
- Liu, T., Semin, B., Klotz, L., Godoy-Diana, R., Wesfreid, J.E. & Mullin, T. 2021 Decay of streaks and rolls in plane Couette-Poiseuille flow. *J. Fluid Mech.* 915, A65.
- Lu, J., Tao, J., Zhou, W. & Xiong, X. 2019 Threshold and decay properties of transient isolated turbulent band in plane Couette flow. Appl. Math. Mech. 40, 1449–1456.
- Packard, A. & Doyle, J. 1993 The complex structured singular value. *Automatica* 29 (1), 71–109.
- Prigent, A., Grégoire, G., Chaté, H., Dauchot, O. & van Saarloos, W. 2002 Large-scale finite-wavelength modulation within turbulent shear flows. *Phys. Rev. Lett.* 89, 014501.
- Prigent, A., Grégoire, G., Chaté, H. & Dauchot, O. 2003 Longwavelength modulation of turbulent shear flows. *Physica. D* 174 (1), 100–113.
- Rabin, S. M. E., Caulfield, C. P. & Kerswell, R. R. 2012 Triggering turbulence efficiently in plane Couette flow. *J. Fluid Mech.* 712, 244–272.
- Schneider, T. M., Gibson, J.F. & Burke, J. 2010 Snakes and ladders: Localized solutions of plane Couette flow. *Phys. Rev. Lett.* **104** (10).
- Tao, J. J., Eckhardt, B. & Xiong, X. M. 2018 Extended localized structures and the onset of turbulence in channel flow. *Phys. Rev. Fluids* 3, 011902.
- Trefethen, L. N., Trefethen, A. E., Reddy, S. C. & Driscoll, T. A. 1993 Hydrodynamic stability without eigenvalues. *Science* 261 (5121), 578–584.
- Tuckerman, L. S. & Barkley, D. 2011 Patterns and dynamics in transitional plane Couette flow. *Phys. Fluids* 23 (4), 041301.
- Tuckerman, L. S., Chantry, M. & Barkley, D. 2020 Patterns in wall-bounded shear flows. *Annu. Rev. Fluid Mech.* 52 (1), 343–367.
- Tuckerman, L. S., Kreilos, T., Schrobsdorff, H., Schneider, T. M. & Gibson, J. F. 2014 Turbulent-laminar patterns in plane Poiseuille flow. *Phys. Fluids* 26 (11), 114103.
- Weideman, J. A. & Reddy, S. C. 2000 A MATLAB differentiation matrix suite. ACM Trans. Math. Softw. 26 (4), 465–519.
- Xiao, X. & Song, B. 2020 The growth mechanism of turbulent bands in channel flow at low Reynolds numbers. J. Fluid Mech. 883, R1.